An Effective, Economic, Aspirated Radiation Shield for Air Temperature Observations and Its Spatial Gradients

CHRISTOPH K. THOMAS AND ALEXANDER R. SMOOT

College of Earth, Ocean, and Atmospheric Sciences, Oregon State University, Corvallis, Oregon

(Manuscript received 1 March 2012, in final form 24 October 2012)

ABSTRACT

This paper presents the design and evaluates the performance of a double-walled electrically aspirated radiation shield for thermometers measuring air temperature and its gradients in the atmospheric surface layer. Tests were performed to quantify its solar radiation error and wake production, and to characterize the observer effect of the forced aspiration on vertical temperature gradients in the calm and stable boundary layer. Construction requirements were to design a unit that uses inexpensive off-the-shelf components, to assemble easily, to facilitate reconfiguration to accommodate various sensors, and to reduce power consumption with the goal of reducing costs and enabling use in sensor networks in remote locations. The custom-aspirated shield was evaluated in reference to a triple-walled commercially available model and subjected to rigorous testing in a wind tunnel and field experiments.

The relative radiation error of air temperature measurements in the custom-aspirated shield was equal to or smaller than that in the reference shield within ± 0.08 K for solar irradiances ≥ 1000 W m^{-2} and calm winds. At night, thermal imagery revealed no significant differences in surface temperatures of both shields and the air temperature. Both shields produced significant wake within a $\pm 30°$ sector of incident flow. Even for weak flows ≤ 0.7 m s^{-1}, higher-order moments were increased by a factor of 3, while the mean airflow speed was reduced by up to 30% compared to uncontaminated directions. Careful inspection of the spatiotemporal dynamics of air temperatures in a vertical profile showed negligible impact of the forced aspiration on the finescale structure of the observations for the nocturnal and transitional calm surface layers.

1. Introduction

Air temperature is of central importance to studies investigating the heat transfer in the natural and built environments, including atmosphere–vegetation interactions, land and sea surface energy exchange, weather forecasting, and climate change science. The temperature of a fluid or object indexes its thermal energy, and in reference to its environment, is a measure of its ability to communicate this energy to other fluids or objects in the form of heat. Since one's ability to accurately measure air temperature and precisely determine its spatiotemporal gradients is directly related to the uncertainty of the analyses employing the air temperature observations, the design and evaluation of air temperature sensors have received much attention in the literature. For surface meteorology applications, it is customary to place the air temperature sensing element, that is, the thermometer, in a protective enclosure to (i) prevent mechanical damage by excessive momentum transfer and objects suspended in the flow during strong winds, and other external influences, such as animals; (ii) keep the sensor surface dry to prevent errors arising from the wet-bulb depression; (iii) prevent the accumulation of particulate matter and development of biofilms that may change the sensor's physical properties, such as diameter, time constant, and reflectivity; and (iv) minimize the radiation error. As the latter typically dominates the overall measurement uncertainty except for very fine-wire sensors, the enclosures are often termed radiation shields, while they also serve the other purposes.

The basic types of radiation shields are stacked plates and concentric tubes that are either naturally ventilated (NatVent) or employ forced aspiration using electric fans. Naturally ventilated radiation shields are typically more economic and require no electric power for aspiration, which is beneficial for sensor networks consisting of multiple stations in remote locations. Much attention

Corresponding author address: Christoph Thomas, Biometeorology Group, College of Earth, Ocean, and Atmospheric Sciences, Oregon State University, 104 CEOAS Admin. Bldg., Corvallis, OR 97331.
E-mail: chthomas@coas.oregonstate.edu

DOI: 10.1175/JTECH-D-12-00044.1

has been devoted to characterizing the airflow (Lin et al. 2001a), radiative regime (Richardson et al. 1999; Lin et al. 2001b), and different coatings (Fuchs and Tanner 1965) on the energy balance of naturally ventilated shields, which may lead to significant errors in air temperature measurements of 2–8 K under weak winds ≤ 1 m s^{-1} and high solar irradiance ≥ 800 W m^{-2} (e.g., Fritschen and Gay 1979; Tanner et al. 1996; Anderson and Baumgartner 1998; Hubbard et al. 2001; Nakamura and Mahrt 2005; Mauder et al. 2008). Some progress has been made to model the energy balance of naturally ventilated radiation shields with the goal of correcting for the radiation error in postprocessing using concurrent measurements of wind speed and shortwave and longwave radiative fluxes outside the radiation shield (Anderson and Baumgartner 1998; Nakamura and Mahrt 2005; Mauder et al. 2008). A recent study by Kurzeja (2010) proposed an approach that does not rely on concurrent measurements but is based on the use of temperature sensors of different diameter to estimate the radiation error. However, significant uncertainty remains for air temperature measurements in naturally ventilated shields even after careful correction arising from (i) assumptions of airflow efficiency (Lin et al. 2001a), which is defined as the ratio between the airspeed inside the shield and wind speed outside the shield; (ii) shortwave radiation penetration ratios into the shield (Richardson et al. 1999); (iii) simplifications built into shape factors representing the shield geometry (Anderson and Baumgartner 1998; Mauder et al. 2008); and (iv) accuracy and representativeness of meteorological input variables and other assumptions, such as standardized measurement height required in corrections (Nakamura and Mahrt 2005). The latter is of particular importance for sensor networks deployed in mountainous terrain and landscapes characterized by vegetation cover of varying density and architecture, such as open forests and savannas, which do not allow for straight-forward modeling of the radiative fluxes and wind speeds because of their large variability in wind, radiation, and thermal microclimates on scales of less than tens or hundreds of meters (Whiteman 2000; Mahrt 2006). In such cases, the remaining uncertainty in air temperature measurements can amount to several tenths in kelvins and thus equate to or exceed the magnitude of the spatiotemporal gradients of interest (Thomas 2011).

Although the use of radiation shields with forced aspiration avoids or significantly reduces these air temperature errors, the costs for commercially available types are prohibitive and often exceed those of the thermometer by far. This may be of particular concern for the growing number of surface meteorology microscale networks dedicated to studying the spatial structure of wind, air temperature and humidity, and snow (e.g., Mahrt et al. 2009, and references therein) as costs grow linearly with the number of stations. Additional concerns are associated with the need for electric power of typically 5–20 W per aspirated radiation shield, the sampling of greater volumes for weak winds compared to naturally ventilated shields, and the alteration of the airflow around the air intake and exhaust. The latter has been speculated to introduce an observer effect by breaking up the finescale structure of stably stratified flows through turbulent mixing induced by the fan (Fritschen and Gay 1979; Kurzeja 2010).

In this study, we propose the design of an aspirated shield that addresses the concerns listed above with the intention of reducing the uncertainty in air temperature measurements and its spatiotemporal gradients by promoting the use of aspirated shields in micrometeorological, ecological, and hydrologic micronetworks. The specific goals were to construct and evaluate a radiation shield whose (i) construction is simple, fast, and uses only economic off-the-shelf components to keep costs at a minimum; (ii) radiation error is similar or better than those of most commercially available shields; (iii) design is flexible enough to accommodate a variety of sensor shapes, sizes, and applications; and (iv) impact on the flow and thermal structure of the air around the sensor is known, particularly for weak wind flows and stable stratification.

2. Theory of radiation error

The theoretical and analytical concept used to quantify the radiation error applies to both naturally ventilated and aspirated radiation shields alike. Both the thermometer and the radiation shield, like any other object, exchange energy with their environment via radiation and convection. Here, conduction through the wall of the sensor housing is assumed to be negligible because of the low thermal conductivity of its material and the small thermal gradients between where the sensor mounts to the radiation shield and the temperature sensing element. In equilibrium with its environment and assuming a dry surface, any excess or deficiency of radiative energy must be balanced by convective sensible heat exchange, so that

$$R_n + H = 0, \tag{1}$$

where R_n is the net radiation balance and H is the convective sensible heat transfer. Substituting parameterizations for both terms and differentiating between shortwave, solar, and longwave, terrestrial radiation yields (Schwerdtfeger 1976; Fritschen and Gay 1979)

$$\left(\frac{1-\overline{\rho_s}}{2}\right)\left(\frac{2K\downarrow}{\pi}+K_d+K\uparrow\right)+\frac{1}{2}(I\downarrow+I\uparrow-2\epsilon_s\sigma T_s^4)+h(T_s-T_a)=0, \quad (2)$$

where $\overline{\rho_s}$ is the average reflection coefficient for shortwave radiation of the surface [1]; $K\downarrow$ is the direct beam and K_d is the diffuse downwelling shortwave irradiance (W m^{-2}); $K\uparrow$ is the reflected shortwave irradiance; $I\downarrow$ and $I\uparrow$ are the downwelling and upwelling longwave irradiances, respectively (W m^{-2}); ϵ_s is the average emission coefficient for the longwave radiation of the surface [1]; σ is the Stefan–Boltzmann constant (W m^{-2} K^{-4}); h is the convective heat transfer coefficient (W m^{-2} K^{-1}); T_s is the surface temperature (K), and T_a is the true air temperature (K). In this general formulation of the heat budget, the subscript s stands for the surface of interest, so either the surface of any of the concentric tubes of the radiation shield or the sensing element. A more explicit model of the sensor's heat budget would need to consider the transfer from the outer to the inner tube, from the inner tube to the sensor's protective housing, and from the protective housing to the sensing element, which is outside the scope of this study. In the case of the outermost tube of the radiation shield exposed to the environment, maximizing the reflection and emission coefficients of the exterior surface reduces R_n since a minimum amount of energy is absorbed, which must then be dissipated. The convective heat exchange depends on the wind speed of the airflow around it, since $h \propto \mathrm{Nu} \propto \mathrm{Re}^m \propto U^m$ with $m \leq 0.5$ (e.g., King 1914), where Nu and Re are the Nusselt and Reynolds numbers, respectively; and U is the total resultant wind speed, defined as $U = (u^2 + v^2 + w^2)^{1/2}$, where u, v, and w are the along-, cross-, and vertical wind components, respectively. For low wind speeds and large solar heating, the heat transfer of the outermost radiation shield may approach free convective conditions, which leads to $h \propto \mathrm{Pr}_t^n$ with $n \leq 0.5$, where Pr_t is the turbulent Prandtl number (e.g., Bejan 2004). In case of the inner radiation shields or the sensor exposed to the inside of the radiation shield, the impact of shortwave radiation is minimized by careful design, that is, $K\downarrow = K_d \approx 0$ W m^{-2}, which leaves the longwave radiative and convective heat transfers as the dominating terms. Low emission coefficients reduce the energy transferred radiatively between the surfaces; the forced aspiration of the inside of the shield and the thermometer at an airflow rate typically $\geq$2.5 m s^{-1} maintains an efficient convective heat transport and helps eliminate temperature differences between the air, the sensor, and the inside of the shield. A statistical evaluation of the surface temperature T_s of the radiation shields is presented in section 4a.

In summary, an air temperature measurement employing an aspirated radiation shield minimizes the radiation error by minimizing R_n and maintaining a sufficiently large h independent of environmental conditions. Air temperature measurements using naturally ventilated radiation shields can minimize the radiation error only be reducing R_n through design, while only limited control over h can be exerted by selecting a sensor with a small diameter d, since $h \propto \mathrm{Nu}\ d^{-1} \propto \mathrm{Re}^m\ d^{-1} \propto d^{(m-1)}$. However, designing a naturally ventilated radiation shield that minimizes R_n by reducing any K term in Eq. (2) inevitably leads to small airflow efficiency and speed inside the shield.

3. Design

We selected a design based on a simple single-walled predecessor model made from polyvinyl chloride (PVC) pipe (H.-P. Schmid 2010, personal communication). The objective was to create a radiation shield whose design would require only inexpensive, easily obtainable materials. A list of materials used in the construction can be found in Table 1 with conversions from metric to imperial units given in Table 2. The construction of the custom-aspirated shield (CAS) required three steps: (i) building a double-walled shield using sections of concentric PVC pipe, (ii) building an aspirator unit, and (iii) connecting the aspirator unit to the shield while allowing air to flow past the sensor at a sufficient flow rate.

a. Shield chamber

The shield construction employs two 0.153-m (6 in.) lengths of 0.042-m outer diameter [1¼-in. nominal pipe size (NPS)] class 200 PVC pipe and one 0.145-m (5¾ in.) length of 0.033-m outer diameter (1-in. NPS) class 200 PVC pipe. Each length of pipe has a 45° cut at one end. The 0.033-m (1-in. NPS) pipe is secured inside one of 0.042-m (1¼-in. NPS) pipe length using wooden dowels (Figs. 1a,b). PVC cement is used to bond the two pieces of 0.042-m (1¼-in. NPS) PVC at their angled ends to form the 90° construction (Fig. 1b). To ensure a maximum surface reflection coefficient, white glossy paint is applied to the outside of the pipe construction. Finally, in order to prevent contact between the sensor and the walls of the shield and thus heat conduction, straws are glued to the inside of the inner shield to support the sensor housing (Fig. 1c).

b. Fan assembly

The source of the aspiration on the CAS design is a 0.06-m, 12-V direct current (dc) fan (see Table 1),

TABLE 1. Part list for CAS construction. See Table 2 for conversion of NPS into metric units. PVC fittings are schedule 40. PVC pipe and fittings can be purchased from plumbing or irrigation suppliers. USD = U.S. dollars.

No.	Description	Quantity	Manufacturer	Cost (USD)
1	1-in. NPS class 200 PVC pipe	1 m	Ridgeline Pipe	1.99/3 m
2	1¼-in. NPS class 200 PVC pipe	0.3 m	Ridgeline Pipe	3.79/3 m
3	1¼-in. NPS PVC 45° wye	1		6.87
4	1¼–½-in. NPS PVC reduced bushing	1		1.41
5	1¼–1-in. NPS PVC reduced bushing	1		1.41
6	1½–1-in. NPS PVC reduced bushing	1		1.48
7	3–1½-in. NPS PVC bell reducer	1		6.52
8	0.0024-m-thick (3/32 in.) polycarbonate sheet	1		7.75/sheet
9	12-V-dc fan 0.060 m × 0.025 m, model 622HH	1	ebm-papst	22.55
10	0.0016-m (0.063 in.)-diameter welded finger guard	1	ebm-papst	3.38
11	0.05 × 0.0064-m (2 in. × ¼ in.) dowel	6		<1.00
12	Machine screw and nut	4		5.26/100
13	Wood screw	4		1.21/10
14	0.15-m (6 in.) plastic drinking straw	2		<1.00
			Total	≈50.00

mounted to a schedule-40 PVC reduced coupling. To mount the coupling, it is necessary to fabricate a disk-shaped mounting plate from a sheet of polycarbonate (Fig. 1d). The fan and finger guard are mounted to the mounting disk using machine screws with the wire leads fed through a hole in the plate (Fig. 1e). The mounting disk is then fixed to the bell reducer with the fan on the inside (Fig. 1f).

c. Main assembly

The shield and fan components were joined to construct the final assembly (Fig. 1g). To fit the sensor securely into the 0.042-m (1¼-in. NPS) to 0.021-m (½-in. NPS) reduced bushing, the 0.021-m (½-in. NPS) opening was bored out with a Dremel grinder. PVC cement was used to make sure all PVC fittings were secured to each other.

d. Alternative configuration: Vertical profile variant

The design of the custom-aspirated shield was modified for the measurement of air temperature in a vertical profile using thermocouples (Fig. 1h, see section 4c). This construction did not make use of the elbow-shaped design, instead favoring a simpler, straight horizontal sleeve geometry while retaining the double-walled shield. The sensor input needed to be plugged with duct seal to support the thermocouple housing and to ensure that it did not touch the inside of the shield walls. The end of the outer sleeve was cut at a 45° angle to prevent rain from entering the shield.

4. Evaluation and discussion

a. Field experiment to quantify radiation error

The field evaluation of the custom radiation shield was performed using air temperature observations over a period of approximately 20 days between May and August 2011 with the air intake installed at 2-m height above short grass in the flat bottomlands of the Willamette Valley, Oregon. Data from individual periods of 3–5 days were combined to reflect the seasonal changes in solar irradiance and azimuth, surface reflection coefficient as the grass senesces, wind speed, and precipitation. Air temperature measurements were collected using a combined probe (model HMP155A, platinum-wire Pt 100, Vaisala, Helsinki, Finland, the successor to the popular model HMP45C) placed in four different radiation shields: a commercially available triple-walled aspirated shield (model 43502, R. M. Young, Traverse City, Michigan; see Table 3) used as a reference (REF), and three identical double-walled CASs (see Table 3) with the intake pointing in three different directions: north, east, and south, referred to as CAS-N, CAS-E, and CAS-S, respectively. The analog output voltages for air temperature and humidity were recorded using the analog input channels of a sonic anemometer (model 81000VRE, R. M. Young) at a sampling rate of 10 Hz, digitized using the onboard 12-bit analog-to-digital (AD) converter, and

TABLE 2. Specifications for all types of PVC pipe used in the construction of the CAS.

NPS	Category	Outer diameter mm (in.)	Inner diameter mm (in.)	Wall thickness mm (in.)
½	Schedule 40	21.34 (0.840)	15.79 (0.62)	2.77 (0.109)
¾	Class 200	26.67 (1.050)	23.37 (0.92)	1.52 (0.060)
1	Class 200	33.40 (1.315)	29.97 (1.18)	1.60 (0.063)
1¼	Class 200	42.16 (1.660)	37.85 (1.49)	2.01 (0.079)
1	Schedule 40	33.40 (1.315)	26.16 (1.03)	3.38 (0.133)
1¼	Schedule 40	42.16 (1.660)	34.54 (1.36)	3.56 (0.140)

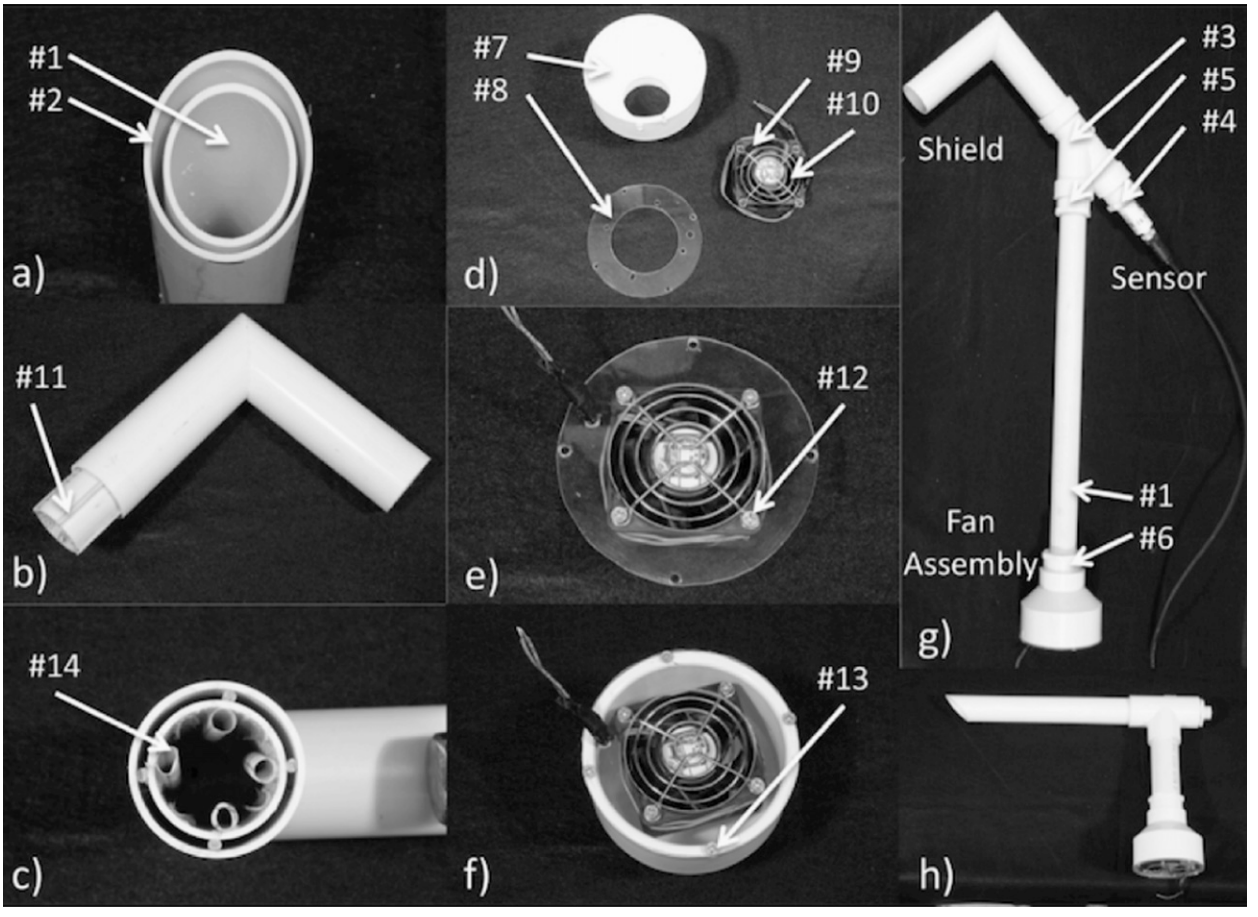

FIG. 1. Double-walled CAS used in this study: (a) shield wall configuration before securing with dowels; (b) shield assembly after cementing 45° edges, and showing how dowels are used to secure inner shield wall; (c) inside of the double shield, note the straws glued to the inside of the walls to separate the sensor housing from the inner wall; (d) components needed for fan assembly; (e) fan attached to mounting plate; (f) completed fan assembly; (g) completed CAS construction with sensor; and (h) variant used for vertical profiling of air temperature using thermocouples (see section 4c). All numbered annotations apply to Table 1.

sent as binary serial string to a datalogger (model CR3000, Campbell Scientific Inc., Logan, Utah) for storage. The measurement resolution of the described sampling and data acquisition system was 0.04 K. The oversampled signals were aggregated to 1-min averages during postprocessing, which corresponds to approximately 2–3 times the time constant of the sensor specified as ≈20–30 s according to the manual. Note that for the purpose of this study, the sintered polytetrafluoroethylene (PTFE) filter protecting the sensing elements was not considered an additional radiation shield when evaluating the radiation error of the aspirated shields. This simplification is justified since the sensor and its housing used in the different radiation shields were identical, and our objective was to construct an inexpensive radiation shield that performs equally or better than commercially available models, and not to comprehensively evaluate the heat budget of the sensor. To account for any systematic biases in air temperature measurements between the sensors in the different radiation shields, a linear regression model was applied to all observations in the CAS. Model coefficients were determined using all nighttime data with wind speeds $U \geq 1$ m s^{-1} when radiation errors and differences between radiation shields are assumed to equal zero. This assumption was verified by measuring the brightness surface temperature of the radiation shields, that is, the emitted infrared radiation, including the air intake using a thermal infrared camera (model SC305, FLIR, Wilsonville, Oregon) as a function of the downwelling shortwave irradiance (Fig. 2). Raw measurements from the camera were corrected for the body temperature of the external optics, the air temperature, and humidity between the camera and the radiation shields; the emissivities of the radiation shields; and reflected surrounding objects. At night when $K\downarrow \approx 0$ W m^{-2}, the surface

TABLE 3. Specifications of commercially available shields and CAS. Met One models 076B-1 and 076B-11 require alternating current (AC); all others use dc power. The flow rate range for the CAS applies to 12–18 V-dc. An image of the CAS is in Fig. 1g. Radiation error for commercially available shields as indicated in the user manual.

Manufacturer and model	Shielding	Power draw (W)	Flow rate (m s^{-1})	Radiation error (K)
R. M. Young 43502	Triple	6–7	5–11	0.2 @ 1000 W m^{-2}
Met One 076B-1	Double	20 (AC)	2.5–5	0.03
Met One 076B-4	Double	3	2.5–5	0.03
Met One 076B-11	Double	18 (AC)	2.5–5	0.03
CAS	Double	2.3	7–10	≤ 0.2 @ 1000 W m^{-2}

temperature of the innermost radiation shield of both the custom-aspirated and reference shields was equal to the air temperature measured by the thermometers for wind speeds $U \approx 1$ m s^{-1}. Downwelling shortwave irradiance was measured using a pyranometer (model PSP, Eppley Laboratory Inc., Newport, Rhode Island) averaged over 1-min increments. Since the objective was to design a radiation shield with an equal or higher efficiency than that of a commercially available reference shield, the relative difference $\Delta T = (T_{CAS} - T_{REF})$ will be used to evaluate the radiation error as a function of shortwave downwelling irradiance and total wind speed according to Eq. (2), where T_{REF} and T_{CAS} are the air temperatures measured inside the reference and custom shields, respectively.

In general, the magnitude of the relative radiation error was very small with $|\Delta T| \leq 0.12$ K (Fig. 3), which corresponds to 3 times the physical measurement resolution and effective uncertainty of the air temperature measurement, $\sigma_{\Delta T}$. The latter is the precision of the measurement setup and was defined as the standard deviation of the temperature differences between air temperature observations in REF and CAS for all nighttime data exceeding $U \geq 1$ m s^{-1} after the application of the linear correction model mentioned above determined at $\sigma_{\Delta T} = 0.04$ K. Some behavior, however, was systematic, albeit its small magnitude and significant scatter. The relative radiation error ΔT was insensitive to the orientation of the CAS for irradiances $K\downarrow \leq 500$ W m^{-2} independent of wind speed. For $K\downarrow > 500$ W m^{-2} and the south-facing CAS, $\Delta T \geq 0$ K and increased with increasing irradiance and decreasing wind speed (Fig. 3c), indicating an equal or higher radiation error for the CAS compared to that of REF. For the highest irradiances and weakest flows, $\Delta T \approx 0.08$ K or $+2\sigma_{\Delta T}$ for CAS-S. The surface temperature of the innermost radiation

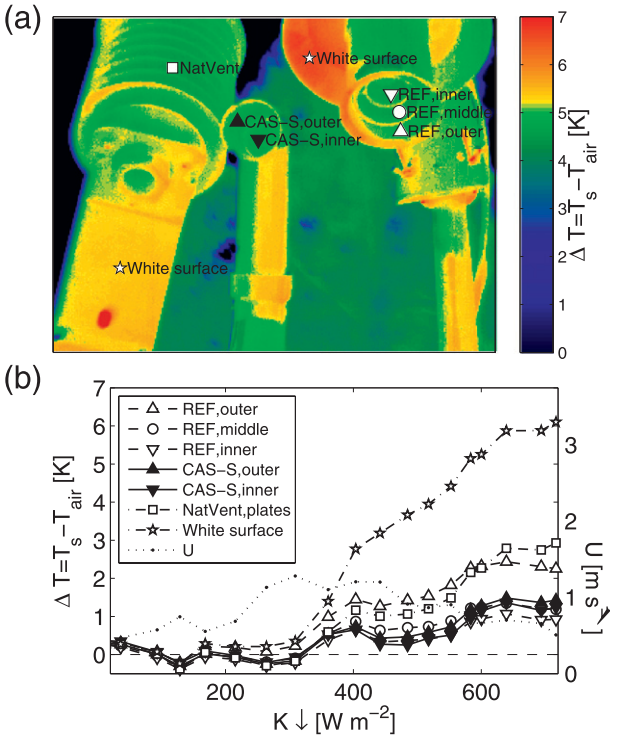

FIG. 2. Surface temperature of the radiation shields: (a) picture of the difference ΔT between brightness temperature, T_s, recorded with a thermal infrared camera and air temperature, T_{air}, observed with the sensors described in section 4a; and (b) ΔT extracted for several regions of interest centered around the indicated markers and total wind speed, U, as a function of downwelling shortwave irradiance, $K\downarrow$, recorded over an 8-h period. CAS is described in section 3, and REF is described in Table 3. For comparison, a multiplated NatVent shield (model 41003, R. M. Young) was included. Images were taken with a camera looking upward into the radiation shields at an inclination angle of ≈45 °.

shield at the air intake measured with the thermal infrared camera was slightly lower for REF than for CAS (Fig. 2b) by about 0.3 K, which supports the finding of the greater radiation error of CAS for this configuration. A direct experimental evaluation of the brightness surface temperature of the temperature sensing element and comparison with the measured air temperature could not be performed because of the shield design, which intentionally obstructs the direct view on the sensor to minimize the amount of shortwave radiation entering the radiation shield. In contrast, $\Delta T \leq 0$ K and decreased with increasing wind speeds and irradiances in case of the north- and east-facing CAS, which indicates an equal or greater efficiency of the CAS compared to REF. Here, efficiency is defined as a shield's ability to minimize the solar radiation error by design and orientation.

The increase in relative radiation error for weaker winds and the south-facing CAS can qualitatively be

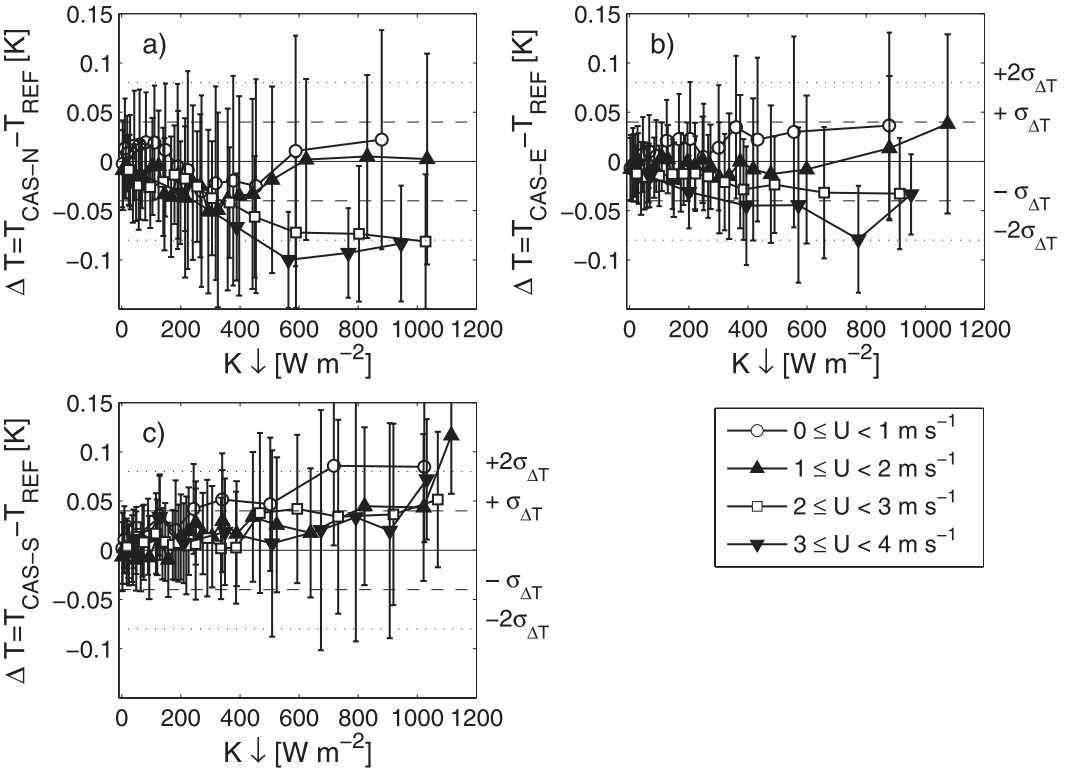

FIG. 3. Daytime relative radiation error ΔT defined as the difference between air temperature observations in the aspirated reference shield, T_{REF}, and those in the CAS with the air intake facing (a) north, $T_{\mathrm{CAS}-N}$; (b) east, $T_{\mathrm{CAS}-E}$; and (c) south, $T_{\mathrm{CAS}-S}$, as a function of downwelling shortwave irradiance, $K\downarrow$, and total wind speed, U. The 1-min observations were aggregated into bins of equal number of data ($N = 150$). The vertical bars represent the standard deviation of observations within each bin. Also shown are multiples of the effective uncertainty or precision of the air temperature measurement, $\sigma_{\Delta T}$, for orientation purposes.

explained by the increased amount of energy absorbed by the single-walled intake of the CAS exposed almost perpendicular to the sunbeams, as $K\downarrow$ has an angular dependence given by the cosine law, and a decrease of the convective heat transfer coefficient on the exterior surface of the shield. Both effects act to increase ΔT according to Eq. (2). In contrast, the decreased relative efficiency of REF with wind speeds ≥ 2 m s^{-2} compared to the east- and north-facing CAS is counterintuitive and requires further investigation. One possible explanation is the orientation of the CAS relative to the wind direction, which, for a specific geometry, may further increase h and thus decrease ΔT, enhancing the efficiency of the CAS beyond that of REF. Stronger winds were oriented primarily perpendicular to the north-facing CAS, maximizing the surface area exposed to the wind and thus h, which results in $\Delta T \approx -0.08$ K or $-2\sigma_{\Delta T}$. This conclusion was supported by the wake analysis in the wind tunnel presented in the next section. The design of the REF shield is omnidirectional, and thus the radiation error is not expected to show any dependence on the direction of the flow.

b. *Wind tunnel experiment to quantify wake production*

Studies investigating the atmospheric heat transport often require closely collocating wind and air temperature sensors to simultaneously observe the spatiotemporal dynamics of the flow and scalar fields, such as estimating spatial gradients, perturbations, and advection. If time scales on the order of minutes, that is, larger than those of turbulence, are of primary interest, then this is often accomplished by pairing sonic anemometers and thermometers with time constants on the order of tens of seconds housed in radiation shields. Such a setup requires careful evaluation, since the radiation shield may induce significant wake, affecting the flow statistics when installed in close proximity to the anemometer. However, stratified flows with small-scale motions prevalent in stable and weak wind boundary layers, for example, flows over ice, snow, and vegetated surfaces without significant mesoscale forcing, require both sensors to be mounted at the same height and at a small horizontal separation distance to physically sample the

same air volume. For evaluation of the impact, one sonic anemometer in combination with a thermohygrometer housed in a REF and one using a CAS were placed side by side at the end of the 10-m free-stream section of a wind tunnel with a cross section of 1.5 m × 1.5 m (Fig. 4). The sampling protocol was identical to that described in the previous section. The onboard head correction reducing the effect of the flow distortion introduced by the support struts was enabled. The center of the sonic anemometer paths was vertically aligned with the air intake of the radiation shields at 0.8 m above the tunnel floor and horizontally separated by 0.35 m. The sensors were mounted on a rotating baseplate to facilitate adjusting their orientation relative to the incident flow. Statistics were computed using the recorded 10-Hz samples over a 3-min period for the positions of ±45°, ±30°, ±15°, ±7.5°, and 0° at the airflow speeds of 0.7, 1.5, 3.4, and 6 m s^{-1}. The position of 0° refers to a configuration when the along-wind component of the airflow, the radiation shield, and the sonic anemometer are aligned (see configuration in Fig. 4). Since the CAS has a directional design, two different spatial configurations were tested: in the tangential configuration, the center line of the radiation shield was perpendicular to the line extending from the center to the support struts of the sonic anemometer when viewed from above, while both were exactly aligned in the case of the radial configuration.

In general, the presence of the radiation shields significantly affected the flow statistics computed from the sonic anemometer data irrespective of airflow speed, CAS configuration, and type of radiation shield. The magnitude of the artifacts introduced by the radiation shields was proportional to the magnitude of the airflow speed in a nonlinear fashion, yielding the greatest relative increase, from 0.7 to 1.5 m s^{-1}. Significant differences were found between REF and CAS, and between the tangential and radial CAS configurations. From this point onward, we will present results for the radial CAS configuration only, since the tangential configuration led to much greater wake production as expected. The magnitude of the total resultant wind vector U was reduced by up to 19% and 28% for the CAS and REF shields, respectively (Figs. 5a,b). Wieser et al. (2001) found similar results studying the flow distortion caused by the transducers and struts alone of a different type of sonic anemometer, but similar geometry compared to that used in this study. The higher-order flow moments, such as the velocity variances and the friction velocity, were increased by a factor of up to 13 and 10 for the CAS and REF shields, respectively (Figs. 5c,d). Minimum ratios of σ_w were observed for the lowest airflow speeds at 0.65 and 0.54 for CAS and REF, respectively (Fig. 5b).

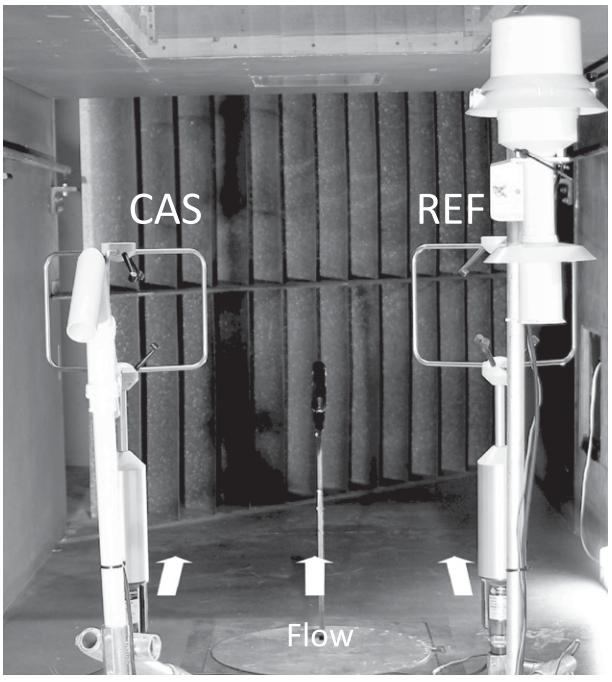

FIG. 4. Picture of the wind tunnel setup to evaluate the wake production of CAS and REF on flow statistics measured with sonic anemometers. The intake of the radiation shields was separated horizontally from the center of the sonic anemometers paths by 0.35 m. The flow was directed into the image. The picture shows the configuration for an incident flow angle of 0°.

In comparison with related studies on the effect of flow obstacles, such as support and tower elements, on flow statistics from sonic anemometers (Grelle and Lindroth 1994; Barthlott and Fiedler 2003; Friebel et al. 2009), the effect of the radiation shields is much larger than those caused by the support struts and transducers alone. The control run, yielding the flow statistics recorded from the sonic anemometer without the presence of radiation shields, yielded an increase of the velocity variances of up to a factor of 2 for an attack angle of 0°, that is, with the flow going through the support strut despite the enabled head correction implemented by the manufacturer, while the magnitude of the mean flow speed was unaffected. The sector of the attack angles parallel to the flow in which statistics were contaminated was relatively narrow within ±30° for both radiation shields, which is in good agreement with similar studies (e.g., Wieser et al. 2001).

c. *Field experiment to assess impact on vertical potential temperature gradients*

The aspiration of the radiation shields leads to sampling of greater air volumes compared to naturally ventilated shields, particularly when the ambient flow is weak and stratified, such as in dense canopies or stable

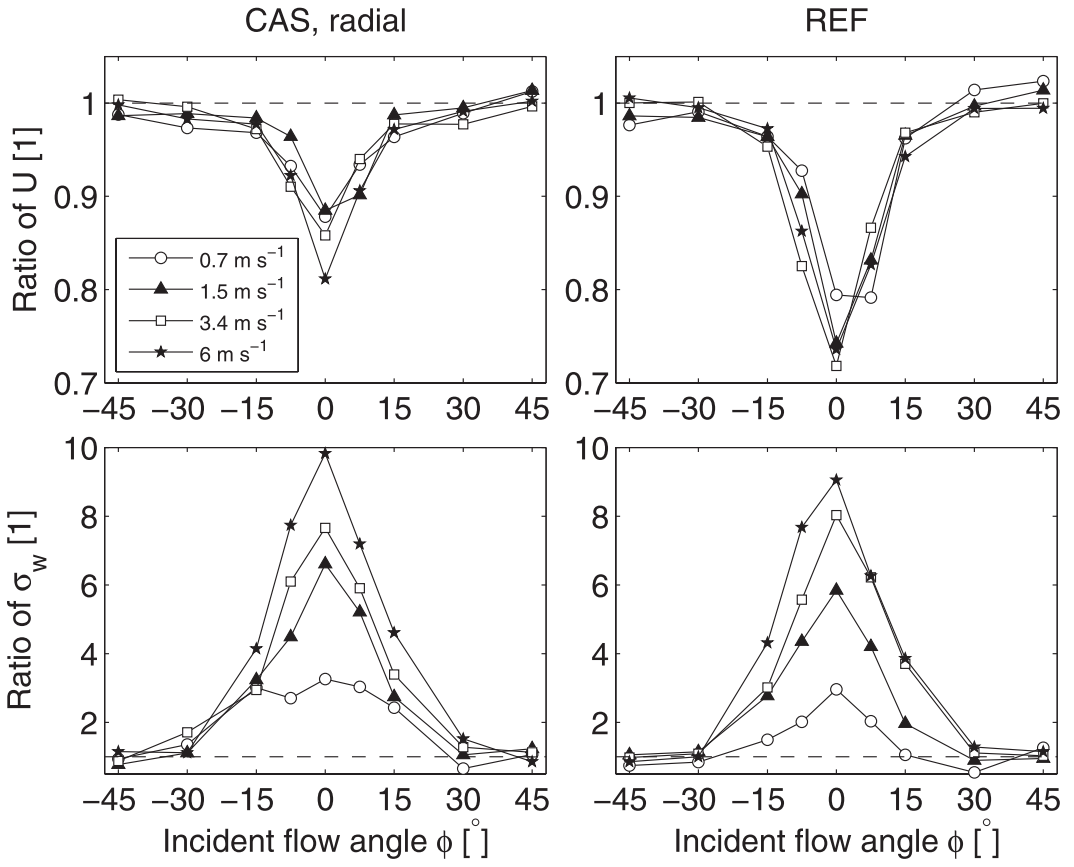

FIG. 5. Ratios of (top) total resultant wind speed $U = (u^2 + v^2 + w^2)^{1/2}$ and (bottom) vertical velocity variance σ_w for incident flow angles $\phi = \pm 45°$, $\pm 30°$, $\pm 15°$, $\pm 7.5°$, and 0° relative to that averaged over those for $\phi = \pm 45°$ for airflow speeds of 0.7, 1.5, 3.0, and 6 m s^{-1} in the wind tunnel for CAS in radial configuration and REF. For details of the setup see section 4b. An incident flow angle of 0° refers to a configuration when the along-wind component of the airflow, the radiation shield, and the sonic anemometer are aligned. The dashed line marks unity.

boundary layers, and to an alteration of the airflow around the air intake and exhaust. Fritschen and Gay (1979) therefore recommended the use of naturally ventilated shields to minimize the observer effect when making observations in these conditions. Kurzeja (2010) compared air temperature observations from naturally ventilated and mechanically aspirated thermocouples in weak airflows with a significant vertical temperature gradient and concluded that the well-mixed air volume sampled with the mechanical aspiration lacks the finescale structure caused by slight fluctuations in streamlines on the order of 0.05–0.10 m. To evaluate the impact of the mechanical aspiration on measuring vertical air temperature gradients and its temporal dynamics, air temperature observations from 12 fine-wire thermocouples (model TMTSS-020, sheath diameter 5×10^{-4} m, Omega Engineering Inc., Stamford, Connecticut) were analyzed. The thermocouples were housed in custom-aspirated shields oriented north–south and installed in a vertical profile at a height of 0.05, 0.10, 0.20, 0.40, 0.80, 1.50, 3.0, 4.0, 6.0, 8.0, 10.0, and 12.0 m above ground level (AGL) over short grass. The thermocouples were interrogated every 2 s using a multiplexer (model AM25T connected to datalogger model CR1000, both Campbell Scientific Inc.) over the period 30 August until 1 October 2011. As a reference, a sonic anemometer was placed at a distance of ≈2 m to the east of the thermocouple profile and thus perpendicular to the predominant flow with its center of the transducers located at 0.8 m AGL. The design of the custom-aspirated shields was slightly modified, such that the double-walled section holding the thermocouple in its center was pointing horizontally to the north with a very short single-walled horizontal drip shield. Because of the close proximity of the lowest three sensors to the surface ground, their aspirating units exhausted horizontally to the south instead of downward.

Ensemble-averaged profiles of potential temperature θ were constructed for two different incident wind direction sectors, light regimes, and wind speed classes

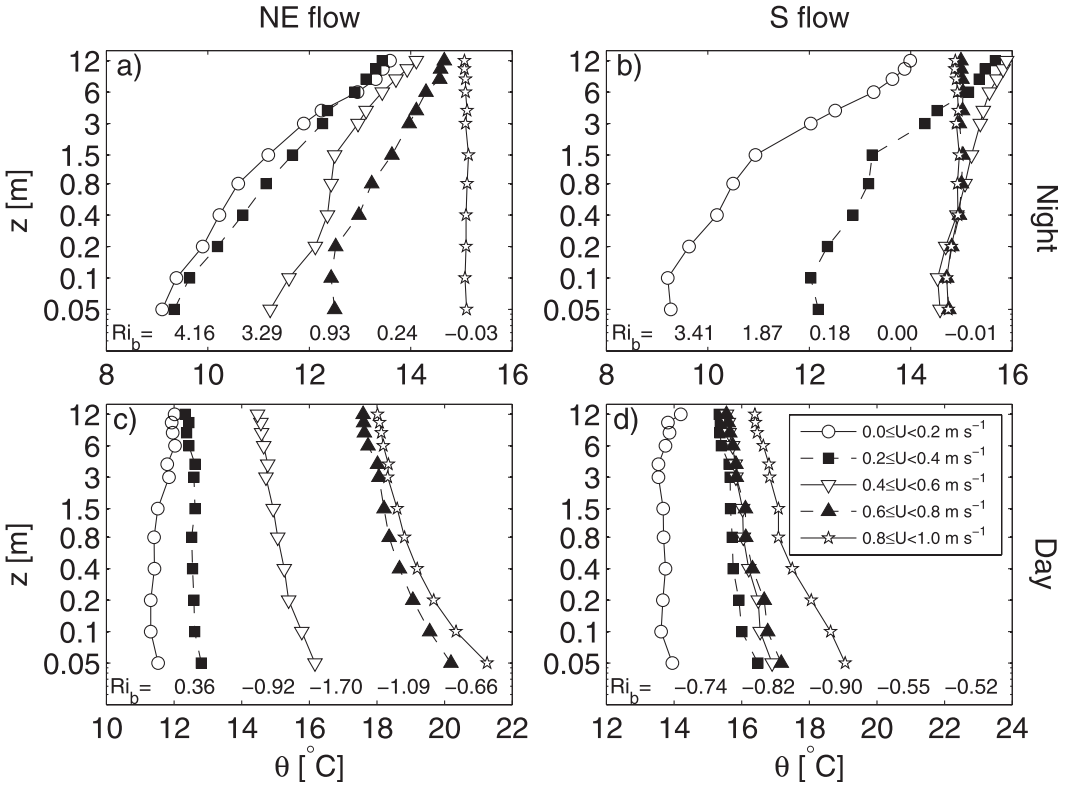

FIG. 6. Ensemble profiles of median potential temperature θ observed using thermocouples situated in CASs for (a),(c) northeasterly (NE) and (b),(d) southerly (S) flow for night and day and different classes of wind speeds (U) observed at 0.8 m AGL. Each profile represents the median of ≥1000 1-min data observed between 28 Aug and 1 Oct 2011. Also noted is the median bulk Richardson number (Ri_b) evaluated between 0.8 and 12 m AGL for wind speed classes in ascending order.

(Fig. 6). At night during weak winds and dynamically stable stratification with bulk Richardson numbers $\mathrm{Ri}_b \geq 1$ when observer effects arising from the mechanical aspiration are expected to be large, the vertical profile of θ resembled the expected logarithmic shape typical of stable boundary layers characterized by a downward transport of sensible heat. The presence of a stationary shallow cold-air pool, which is often observed at this experimental site (Thomas et al. 2012), led to a change in $\partial\theta\ \partial \ln z^{-1}$ at its interface to the warmer overlying air at a height of approximately 1.5 m AGL for $U \leq 0.6$ m s^{-1}. The behavior of the temperature observed with the lowest sensor in relation to the rest of the profile was sensitive to the incident wind direction: for northeasterly flows when the flow was unobstructed and thus not expected to be altered by the aspirator, the mean minimum temperature was observed at 0.05 m and fit well into the logarithmic profile (Fig. 6a). For southerly flows, however, when the sample volume was potentially perturbed by the mechanical aspirator, the minimum temperature was observed at 0.10 m AGL (Fig. 6b). It remains unclear if this anomaly indicates an observer effect caused by the aspiration or a physical signal, as the forced mixing induced by the fans upstream of the thermocouples would act toward eliminating any vertical temperature gradients. During the morning transition, characterized by very weak winds $U \leq 0.2$ m s^{-1} but significant solar irradiance resulting in $\mathrm{Ri}_b \leq -0.3$, the temperature profiles resolved the vertical divergence in sensible heat flux, showing a surface heating and upward heat transport close to the ground but a downward heat transport aloft (Figs. 6c,d). Time series plots of temperature records from the thermocouples and the sonic anemometer revealed a richness in structures across the lower part of the profile for $z \leq 1.5$ m AGL, visible as fast-changing spatiotemporal gradients (Fig. 7). Despite the mechanical aspiration, significant vertical differences and temporal dynamics in traces of potential temperature were conserved, even closely collocated sensors closest to the ground can be distinguished. Fine details, such as a temporary reversal of the vertical temperature gradient between the lowest observation heights of 0.05 and 0.10 m AGL [1925 Pacific standard time (PST)], were observed.

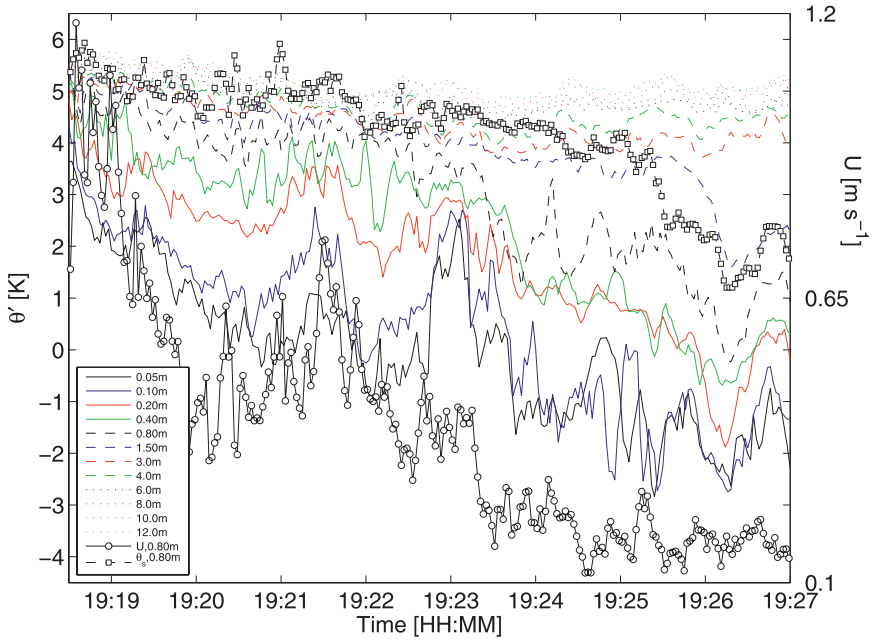

FIG. 7. Time series of potential temperature perturbations from the 30-min temporal mean measured at 0.05 m AGL, θ', observed using fine-wire thermocouples situated in CASs in a vertical profile (lines) over short grass. The temporal resolution is 0.5 Hz. Also shown are the sonic potential temperature, θ_s, and the 1-min-averaged total resultant wind speed, U, observed with a sonic anemometer at 0.8 m AGL laterally separated from the thermocouple profile by ≈2 m perpendicular to the flow.

The comparison of the dynamics of the potential temperature from the thermocouple in the custom-aspirated shield and the speed-of-sound-based temperature from the sonic anemometer at the same height yielded no significant differences in first- and higher-order moments for flows perpendicular to the horizontal separation, which is in contrast with the findings by Kurzeja (2010). Despite the significant horizontal separation of ≈2 m, the signature of transient motions, for example, passing at 1926:30 PST, was registered by both sensors in a very similar fashion, which supports the finding that the aspiration does not significantly perturb the structure of the airflow and its scalar fields.

5. Conclusions

The evaluation of the double-walled custom-aspirated radiation shield led to the following conclusions with respect to the goals of the study listed in the introduction.

- The use of commercially available off-the-shelf irrigation PVC pipe, connectors, and motorized fan reduced the cost per aspirated radiation shield well below a tenth of that of an equivalent commercially available radiation shield. The variety of PVC connectors and pipes allows for easy and inexpensive adjustment of the shield's design to accommodate specific measurement configurations and sensors, such as the vertical profiling described in section 4c. Particularly when many units are made at the same time, the production time can be reduced to about 20 min per unit and manufacturing can be done with simple hand tools, such as cutters, power drill, screw driver, and PVC cement. The electric fan used in our design requires less power than commercially radiation shields, which is important for battery-buffered systems relying on solar power for remote applications.
- Despite the use of inexpensive components, the radiation error for air temperature measurements in the double-walled custom-aspirated shield was less or equal to that in a triple-walled commercially available shield. Note that for the purpose of this study, which aims at devising a practical, economic pathway of reducing the uncertainty in air temperature measurements over existing techniques, we chose a relative measure of the radiation error in comparison with a commercially available product with a known radiation error (0.2 K at 1000 W m^{-2}; see Table 3). While this comparative approach allows for constraining the radiation error of the custom-aspirated shield to <0.2 K, the true air temperature and thus the absolute radiation error of the custom-aspirated shield ultimately

remains unknown because of the inherent difficulties in modeling and measuring air temperature irrespective of the approach.

- The directional design of the custom radiation shield requires the air intake pointing north to achieve a maximum efficiency and reduction of the radiation error.
- The turbulent wake induced by the custom and commercially available aspirated radiation shields is significant and needs to be considered when flow statistics are recorded with a fast-response sensor, such as a sonic anemometer in close proximity. The radiation shields reduce the mean speed of the flow but inflate high-order statistics, such as velocity variances and momentum transport, by up to a factor of 20 compared to unobstructed incident flow directions. The sector of contaminated incident attack angles parallel to the flow is relatively narrow, within ±30°. Even for weak flows with $U \leq 0.7$ m s^{-1}, data from these sectors need to be excluded from analysis.
- The mechanically forced aspiration had a negligible impact on the spatiotemporal dynamics of air temperature observations and its gradients even under conditions of weak flows and stable stratification. Despite the greater sampling volume, differences in the variety of motions on time scales on the order of seconds to tens of seconds were resolved with two sensors physically located within 0.05 m of each other close to the ground. Nighttime vertical profiles of potential temperature obeyed logarithmic scaling even for weakest flows, with $U \leq 0.2$ m s^{-1} and strongly dynamic stability with $\mathrm{Ri}_b \geq 1$.

Acknowledgments. This research was funded by the National Science Foundation, Award AGS 0955444, ''CAREER: A New Direction into Atmospheric Near-Surface Transport for Weak-Wind Conditions in Plant Canopies.'' We thank James Liburdy for use of the wind tunnel facilities, and Javier Orozco for assisting in collecting of field observations.

REFERENCES

Anderson, S. P., and M. F. Baumgartner, 1998: Radiative heating errors in naturally ventilated air temperature measurements made from buoys. *J. Atmos. Oceanic Technol.,* **15,** 157–173.

Barthlott, C., and F. Fiedler, 2003: Turbulence structure in the wake region of a meteorological tower. *Bound.-Layer Meteor.,* **108,** 175–190, doi:10.1023/a:1023012820710.

Bejan, A., 2004: *Convection Heat Transfer*. 3rd ed. John Wiley & Sons, 694 pp.

Friebel, H. C., T. O. Herrington, and A. Y. Benilov, 2009: Evaluation of the flow distortion around the Campbell Scientific CSAT3 sonic anemometer relative to incident wind direction. *J. Atmos. Oceanic Technol.,* **26,** 582–592.

Fritschen, L., and L. Gay, 1979: *Environmental Instrumentation*. Springer Verlag, 216 pp.

Fuchs, M., and C. Tanner, 1965: Radiation shields for air temperature thermometers. *J. Appl. Meteor.,* **4,** 544–547.

Grelle, A., and A. Lindroth, 1994: Flow distortion by a solent sonic anemometer: Wind tunnel calibration and its assessment for flux measurements over forest and field. *J. Atmos. Oceanic Technol.,* **11,** 1529–1542.

Hubbard, K. G., X. Lin, and E. A. Walter-Shea, 2001: The effectiveness of the ASOS, MMTS, Gill, and CRS air temperature radiation shields. *J. Atmos. Oceanic Technol.,* **18,** 851–864.

King, L., 1914: On the convection of heat from small cylinders in a stream of fluid: Determination of the convection constants of small platinum wires, with applications to hot-wire anemometry. *Philos. Trans. Roy. Soc. London,* **A214,** 373–432.

Kurzeja, R., 2010: Accurate temperature measurements in a naturally-aspirated radiation shield. *Bound.-Layer Meteor.,* **134,** 181–193, doi:10.1007/s10546-009-9430-2.

Lin, X., K. G. Hubbard, and G. E. Meyer, 2001a: Airflow characteristics of commonly used temperature radiation shields. *J. Atmos. Oceanic Technol.,* **18,** 329–339.

——, ——, and E. A. Walter-Shea, 2001b: Radiation loading model for evaluating air temperature errors with a non-aspirated radiation shield. *Trans. ASAE,* **44,** 1299–1306.

Mahrt, L., 2006: Variation of surface air temperature in complex terrain. *J. Appl. Meteor. Climatol.,* **45,** 1481–1493.

——, C. Thomas, and J. Prueger, 2009: Space-time structure of mesoscale modes in the stable boundary layer. *Quart. J. Roy. Meteor. Soc.,* **135,** 67–75.

Mauder, M., R. L. Desjardins, Z. Gao, and R. Van Haarlem, 2008: Errors of naturally ventilated air temperature measurements in a spatial observation network. *J. Atmos. Oceanic Technol.,* **25,** 2145–2151.

Nakamura, R., and L. Mahrt, 2005: Air temperature measurement errors in naturally ventilated radiation shields. *J. Atmos. Oceanic Technol.,* **22,** 1046–1058.

Richardson, S. J., F. V. Brock, S. R. Semmer, and C. Jirak, 1999: Minimizing errors associated with multiplate radiation shields. *J. Atmos. Oceanic Technol.,* **16,** 1862–1872.

Schwerdtfeger, P., 1976: *Physical Principles of Micrometeorological Measurements.* Developments in Atmospheric Science, Vol. 6, Elsevier Scientific Publishing Company, 113 pp.

Tanner, B., E. Swiatek, and C. Maughan, 1996: Field comparison of naturally ventilated and aspirated radiation shields for weather station air temperature measurements. Preprints, *22nd Conf. on Agricultural and Forest Meteorology,* Atlanta, GA, Amer. Meteor. Soc., 227–230.

Thomas, C. K., 2011: Variability of sub-canopy flow, temperature, and horizontal advection in moderately complex terrain. *Bound.-Layer Meteor.,* **139,** 61–81, doi:10.1007/s10546-010-9578-9.

——, A. M. Kennedy, J. S. Selker, A. Moretti, M. H. Schroth, A. R. Smoot, N. B. Tufillaro, and M. J. Zeeman, 2012: High-resolution fiber-optic temperature sensing: A new tool to study the two-dimensional structure of atmospheric surface-layer flow. *Bound.-Layer Meteor.,* **142,** 177–192, doi:10.1007/s10546-011-9672-7.

Whiteman, C. D., 2000: *Mountain Meteorology*. Oxford University Press, 355 pp.

Wieser, A., F. Fiedler, and U. Corsmeier, 2001: The influence of the sensor design on wind measurements with sonic anemometer systems. *J. Atmos. Oceanic Technol.,* **18,** 1585–1608.